This manuscript has been accepted for publication in the Proceedings of the 43rd IEEE Photovoltaic Specialists Conference, held in June 5-10, 2016, in Portland, Oregon.

Multi-year Ground-based Irradiance Dataset in a Northern Urban Climate

J. E. Haysom, P. McVey-White, L. de la Salle, K. Hinzer and H. Schriemer

SUNLAB, University of Ottawa, Ottawa, ON, K1N 6N5, Canada

***Abstract* — A multi-year irradiance dataset has been collected using secondary standard pyrheliometer and pyranometers at a Canadian urban test site. Detailed screening algorithms, instrument bias corrections, and uncertainty analyses were undertaken to produce a high accuracy, validated dataset for global horizontal irradiance (GHI), direct normal irradiance (DNI) and diffuse horizontal irradiance (DHI). The inter-comparison of the three instruments is included within a study of the DHI shadowband correction model, and confirms agreement with mean bias errors less than 4%. Comparative studies of measurements with satellite data were undertaken, and the agreement for GHI daily values with NASA satellite data exhibited a relative mean bias error (rMBE) of - 1.7% and a relative root mean squared error (rRMSE) of 24.3%. The agreement for DNI hourly values in comparison to SolarAnywhere v3 was -1.2% with an rRMSE of 8.8%. In all three statistical analyses, the agreements are within the instrumental uncertainty, providing very strong validations of the ground-based dataset and of the accuracy of the satellite-derived data. Frequency distribution versus DNI for ground and satellite data are found to have some differences in-line with the nature of their measurement characteristics.**

***Index words:* direct normal ground irradiance, diffuse shadowband correction, frequency distribution, instrument uncertainty**

I. Introduction

Precise knowledge of the solar resource has become increasingly important in renewable energy and climate change research. Furthermore, solar irradiance maps and geographically extensive datasets have tremendous value in assessing the overall potential for a solar generating facility in a broad range of locations. These datasets and maps employ models to predict the solar resource using either weather station measurements or satellite data [1], and research continues to improve their accuracy and the quantification of that accuracy [2-3]. Such work relies on high-quality ground-based datasets as the "ground truth". These ground-based irradiance measurements must have high standards for instrument cleaning and maintenance, and should include multiple instruments and redundancy [4]. A dataset that contains the direct normal irradiance (DNI), the diffuse horizontal irradiance (DHI), and the global horizontal irradiance (GHI) as separate measurements is desirable. Continuous collection and validation of complete datasets presents a challenge, especially under winter conditions, and particularly for DNI, which requires a high-precision dual-axis sun tracker. Since there are few validated ground-based DNI datasets in many regions of the world, especially in northern climates [5], this work contributes to the world body of solar resource data. The paper is devided into five sections. Section II describes the instruments in detai, and explains the data validation process. Section III examines the shadowband correction model for the DHI dataset and instrument intercomparision. Section IV contains comparitive analysis of the GHI and DNI dataset to satellite measurements, and Sections V and VI contain discussion and conclusions.

TABLE I
SUNLAB TEST SITE EQUIPMENT SPECIFICATIONS
* indicates mounted on tracker

Instrument	Manufacturer	Specification	Installed
Dual-axis tracker	GoldenSun	0.1° – 0.2° acc.	Jan 2011
NIP pyrheliometer	Eppley*	285-2800nm	March 2011
PSP pyranometer with ventilator	Eppley	285-2800nm	March 2011, XXX 2013
PSP pyranometer, shadow band, no ventilator	Eppley	285-2800nm	July 2013
Spectroradiometer	ASD inc*	350-1830nm, 3nm resolution	April 2011
SolarSIM spectral irradiance meter	Spectrafy*	280-4000nm, 1nm resolution	Sept 2013
CCD Camera pointed at the sun	Vivotek*	Approximately 3° FOV	Jan 2011
WS501 Weather station	Lufft	Pressure, temperature, humidity, wind speed and direction, and GHI (300-1100nm)	Sept 2013

II. Quality Control of Ground Measurements

The SUNLAB deployed a solar test site in Ottawa, Canada (Lat: 45.42, Long: -75.69, elevation 70 m) in 2011 [6] to undertake research on flat plate photovoltaics (PV), concentrated photovoltaics (CPV), and the effects of atmospheric constituents on the solar spectrum. The instrumentation includes secondary standard thermopile irradiance sensors, weather sensors, and spectral measurements - a detailed instrumentation list is presented in Table I. This paper will focus on data from the three Eppley thermopile radiometers collected between October 2012 and Dec 2015; the spectral instruments are discussed and cross-compared elsewhere [7]. The instruments are cleaned weekly and measurements taken on 2 minute timestamps. Post-processing of data from the pyranometers and pyrheliometer is

critical to ensure that the GHI, DHI, and DNI measurements are accurate and representative. Methodologies for calibration correction, uncertainty analyses, and data screening are explained in this section.

A. Temperature and cosine response calibration correction

A Campbell Scientific CR1000 Measurement and Control Datalogger collects raw voltage measurements from the pyranometers and the pyrheliometer. Radiative powers are then calculated using the instrument's calibrated responsivity constant and further adjusted using a polynomial fit to the temperature dependent curve, as provided by the manufacturer.

Pyranometer responsivity is known to have a small deviation from the cosine relationship with beam power due to high-angle reflectivity losses and other secondary effects. Reda provides a curve of this cosine error for an Eppley PSP pyranometer during a clear sky day [8]. We take a polynomial fit of this curve and use it to correct all GHI data, not just the clear sky data. Although some residual inaccuracy in the correction will therefore remain, it will mostly be for periods of low irradiance. We believe this method provides an improved linearity overall to the dataset, as further discussed below.

B. Uncertainty Analysis

Each element of the calibration and measurement system contributes to the overall uncertainty in the final values. In this work, the methodologies explained in [4] and [9] have been followed to determine the expanded uncertainty, U_E. Type A sources, $u_{i(A)}$, originating from statistical variability, and Type B sources, $u_{i(B)}$, originating from product specification and other evaluations of precision, are itemized for each of the three instruments in Table II. The first six rows are taken from [9] for pyrheliometers and also applied to the pyranometers. One exception, the optical cleanliness for our DHI instrument, is set higher due to the possibility of condensation or ice on the (unvented) dome – the dataset has been filtered for such anomalies but the screening is likely not perfect. Alignment errors for the DNI are the same as in [9], set to zero for the GHI, and estimated to be relatively large for the DHI due to the manual adjustment of the shadowband. The datalogger's specifications and the method in [9] are used to determine the sixth row. Following [8] we estimate that the application of the cosine correction to the GHI has a statistical uncertainty (Type A) of 0.3% and a bias (Type B error) of 1.35%, which is equal to 20% of its full scale range of the experimental curve in [8]. This is smaller than Reda's value of 2.1% if no cosine correction were undertaken. The DHI instrument, though it is not subject to the direct beam cosine error, is still assigned a small error in this category due to variations in the angular distribution of the diffuse irradiance.

For each instrument, the uncertainties are combined to determine the extended uncertainty as follows:

$$TypeA = \left[\sum \left(u_{i(A)}\right)^2\right]^{1/2} \quad (1a)$$

$$TypeB = \left[\sum \left(u_{i(B)}\right)^2\right]^{1/2} \quad (1b)$$

$$U_E = k * \left[\sum (TypeA)^2 + \sum (TypeB)^2\right]^{1/2} \quad (1c)$$

where k is a correction factor that depends on the desired accuracy; we use $k = 1.96$ for a confidence interval of 95% on normally distributed data. These calculations result in expanded uncertainties for U_E of 2.7%, 3.2% and 2.9%, for DNI, GHI, and DHI data, respectively.

C. Tracker screening algorithm applied to DNI

The GoldenSun tracker is a commercial dual-axis tracker with 21 m^2 module capacity. It includes three instruments to monitor position: *Elevation* and *Azimuth* are measured with potentiometers connected to the tracker, while active sun tracking is accomplished with a sun sensor. The latter is a four quadrant sensor, with tracking achieved by minimizing the differential signal between photodiode pairs. Three data streams are available: *East/West Difference*, *North/South Difference*, and *Total Signal*.

We use these five tracker signals in a screening algorithm that rejects data when tracking fails, while accepting zero- and low-DNI data from overcast days. Each timestamp is screened against the following criteria:

1. DNI is between zero and the extra-terrestrial radiation value; AND
2. time is between sunrise and sunset; AND
3. tracker data is available; AND
4. the tracker is operating in closed-loop mode using sun sensor feedback and the sun sensor difference values indicate tracker is aligned; OR
5. the tracker is operating in open-loop mode because the sun sensor's *Total Signal* value is too low, AND *Elevation* and *Azimuth* readings indicate the tracker is aligned.

For criterion 4, "aligned" has been determined by a field test: on a clear sky day, the tracker was moved off sun, and the values of *East/West Difference* and *North/South Difference* when the pyrheliometer signal declined by more than 10% were recorded as the alignment threshold. For criterion 5, under overcast skies (DNI values of approximately ≤ 160 W/m^2) the *Total Signal* is too small and the tracker operates in open loop. Instead of rejecting these low DNI values, our algorithm accepts the timestamp if *Elevation* and *Azimuth* values are within ±2.9^o of calculated sun position. This algorithm has two advantages: first, the DNI dataset will include validated low DNI values; and second, accurate alignment to within the pyrheliometer's field of view is confirmed, eliminating misrepresentative readings.

D. Screening due to test site shadows

The test site is well situated in a location with a good view of the sky dome and an unobstructed southern exposure, however it is still an urban location. The distant horizon includes buildings and trees, causing shadowing for zenith angles approximately ≥ 80°. Westerly university buildings also cast shadows during azimuths > 252° (setting sun in the summer months). Timestamps with these conditions are removed.

E. Statistical Analysis

To assess the agreement between various sources of irradiance data, the relative mean bias error (rMBE) and the relative root mean squared error (rRMSE) are calculated as follows:

$$rMBE = \frac{1}{N}\sum_{n=1}^{N}\left[\frac{X_{n,ground} - X_{n,sim}}{X_{n,ground}}\right], \quad (2)$$

$$rRMSE = \sqrt{\left(\frac{1}{N}\sum_{n=1}^{N}\left[\frac{X_{n,ground} - X_{n,simulated}}{X_{n,ground}}\right]^2\right)}. \quad (3)$$

TABLE II
ESTIMATED UNCERTAINTIES, u (%)

	Type A			Type B		
	DNI	GHI	DHI	DNI	GHI	DHI
Fossilized calibration error	0.615	0.615	0.615	0.665	0.665	0.665
Temperature response	0.25	0.25	0.25	0.25	0.25	0.25
Linearity	0.1	0.1	0.1	0.125	0.125	0.125
Window transmission	0.1	0.1	0.1	0.5	0.5	0.5
Optical cleanliness	0.2	0.2	0.5	0.25	0.25	0.25
E&M interference	0.005	0.005	0.005	0.005	0.005	0.005
Alignment	0.2	0	0.5	0.2	0.05	0.5
Data logger	0.4	0.4	0.4	0.03	0.03	0.03
Cosine	0	0.3	0.2	0	1.35	0.2
Type A and B totals	0.837	0.855	1.068	0.935	1.632	1.060
Expanded Uncertainty	2.7	3.2	2.9			

III. CORRECTION OF DHI DATA FOR SHADOWBAND

The output from the DHI pyranometer with shadowband needs to be upward corrected to account for the blocked portion of the diffuse sky due to the band. A simple geometric correction is insufficient due to the anisotropy of the diffuse sky dome, and several papers have proposed models which are tested using ground data [10]. A recent analysis by Sanchez *et al.* [11] shows that two Batlles models, labelled "BA" and "BB", provided the best fit to ground measurements in Spain [12], and thus they are considered here. The models augment a simple geometric correction factor C_d with three anisotropic correction terms that relate to the brightness index, Δ, the cloud condition, ε, and the zenith angle, Z, as per the following equations:

$$\Delta = DHI_{meas} / (I_o \cos(Z)), \quad (4a)$$

$$\varepsilon = (DNI_{meas} + DHI_{meas}) / DHI_{meas}, \quad (4b)$$

$$DHI_{corr} = DHI_{meas}\,(a_i C_d + b_i \log(\Delta) + c_i \log(\varepsilon) + d_i e^{-1/\cos(Z)}), \quad (4c)$$

where I_o is the extraterrestrial irradiance, and a_i, b_i, c_i, and d_i are four fitting parameters that need to be determined by linear regression using a measured dataset. The BA model considers one expression for all sky conditions (i=1 only), whereas the BB model divides the dataset into four different bins (i=1 to 4) based on sky conditions, with bins defined by the value of ε: $\varepsilon \leq 3.5$, $3.5 \leq \varepsilon \leq 8$, $8 \leq \varepsilon \leq 11$, and $11 \leq \varepsilon$. In the BB model, the c_i parameters, which influence the effect of ε in equation 4(c), are set to zero, and as well, in the two clearest sky conditions, d_3 and d_4 are also set to zero.

Our analysis is undertaken using 2 min timestamps, where the DHI_{corr} from equation 4(c) is compared to a value of DHI, DHI_{calc}, calculated from the two other ground instruments following:

$$DHI_{calc} = GHI_{meas} - DNI_{meas} \cdot \cos(Z) \quad (5)$$

where Z is the solar zenith angle. During the fitting routine, additional data screening is undertaken to remove suspect outlier data: all winter months are avoided due to the potential of frost on instruments, large inter-instrument discrepancies are removed (which may be due to events such as a cloud shadow on one instrument only), resulting in 24,430 timestamps. Statistical assessment is undertaken using (2) and (3), where $DHI_{n,calc}$ is used for $X_{n,ground}$ and $DHI_{n,corr}$ is used for $X_{n,sim}$.

Using the BA model with parameters tuned at a Spanish site [11], we obtain an rMBE of 12.5% and an rRMSE of 19.0%, which are values larger than found in the original study. The larger discrepancy with the Ottawa dataset is thought to be a combination of the need to tune the fit parameters to climatic conditions as well as a systematic disagreement between instruments. We study this by examining data from a representative overcast day (March 26, 2015) and a representative clear sky day (March 28, 2015), as shown in Fig. 1.

Employing linear regression tuning of the fit parameters of the BA model, the rRMSE for the overcast day is reduced to 1.5%. By contrast, a satisfactory fit to the clear sky day is not

obtained due to the dramatic split in morning and afternoon portions of the curve. We assess the poor fit for the clear sky day as being due to instrument design: the pyrheliometer, with an acceptance angle of ±2.9°, will reject the extended angle circumsolar radiation, but the DHI instrument does not collect it since its shadowband has a rejection angle of ±6.5°. Thus, the DHI measured is lower than it should be in nearly clear sky conditions. The magnitude will be influenced by water vapour levels and atmospheric aerosols, the latter of which may vary significantly throughout the day in an urban environment. Thus, urban aerosols and diffuse sky anisotropy challenge the accuracy of a shadowband instrument and its correction model.

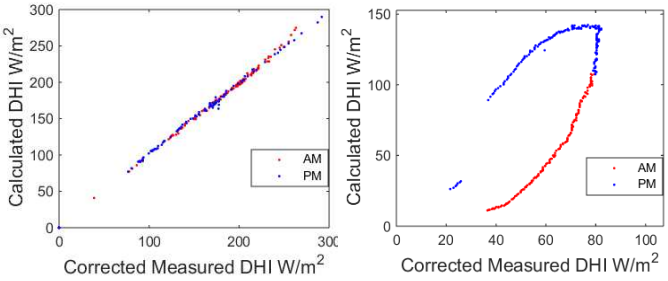

Fig. 1. Scatter plot of 2 min data for the calculated DHI versus the corrected DHI for example days (a) cloudy day and (b) clear sky day. Morning (AM) and afternoon (PM) as per daylight saving time are colour coded red and blue respectively.

To achieve the most accurate correction possible for our dataset over all sky conditions, we choose to employ the BB model including tuning of the fit parameters in each bin. The result is shown in Fig. 2, with statistics presented in Table III. The agreement is quite satisfactory, with the rMBE for each bin in the range from -3.9 to 2.3%, which are within the instrumental uncertainties. As expected from the above analysis, the rRMSE values are lowest in the cloudy sky conditions at 7.62% and worst for the clear-sky conditions at 24.2%. Note that this study also allows us to conclude that, on average, the test site's three instruments are in agreement with each other within their uncertainties.

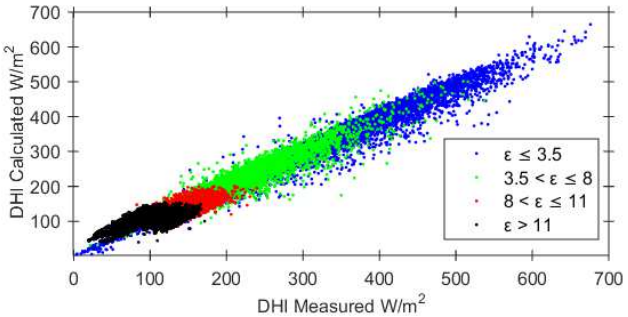

Fig. 2. Scatter plot of 2 min data of calculated DHI versus the tuned shadowband-corrected DHI using the BB model. The four cloud condition bins are each displayed in a different colour as yellow ($\varepsilon \leqslant 3.5$), red ($3.5 < \varepsilon \leqslant 8$), green ($8 < \varepsilon \leqslant 11$) and blue ($\varepsilon > 11$).

TABLE III.
AGREEMENT BETWEEN THE BB MODEL SHADOWBAND CORRECTION FOR DHI AND CALCULATED DHI.

	$\varepsilon \leqslant 3.5$	$3.5 < \varepsilon \leqslant 8$	$8 < \varepsilon \leqslant 11$	$\varepsilon > 11$
rRMSE (%)	7.6	11.0	15.9	24.2
rMBE (%)	2.3	1.3	1.7	-3.9

IV. ANALYSIS OF GROUND VS SATELLITE DATA

The above work provides a well-calibrated and validated ground-measured dataset, but it suffers from two major limitations: (i) it is not a complete (continuous) dataset, thus posing challenges for use in project energy yield predictions, and (ii) it is only representative of one location, thus a wide network of such stations are required for project development across regions. The use of satellite imagery can avoid both of these limitations, but the modeling algorithms should be tuned and tested against validated ground truth data, where possible. In Canada, there are very few sites with ground measured data [13], in particular, sites that measure DNI and that cover the recent time period. In this paper, we undertake a preliminary analysis of the agreement between the GHI and DNI ground and satellite data.

In undertaking these comparisons, it is important to note that satellite data and ground truth data may differ due to several factors: (i) geographic averaging due to the width of the satellite images, (ii) sampling rates, (iii) issues with ground measurement instruments, and (iv) satellite modeling error due to snow cover or other atmospheric input approximations.

A. GHI Data Comparison

Ground measured GHI daily sums were compared with commonly-used and freely available satellite daily sums from NASA [14] for timestamps between Jan 17, 2013 and April 20, 2015 (699 days total). The comparison exhibits an rMBE of - 1.69%, which is within instrumental uncertainty and is in agreement with other industry reports [15]. By contrast, an rRMSE of 24.3% is found, which is at the high range of industry observed values, and is possibly due to the challenges of frost and snow coverage on satellite data extraction. We therefore extend the analysis by grouping the data into two subsets based on clarity index k_t, the fraction of global irradiance over extraterrestrial irradiance. Fig. 3 shows that for low k_t values, NASA data overestimates the ground irradiance with an rMBE of 5.79%, while for high k_t conditions, it underestimates it with an rMBE of -18.77%; these trends are slightly different than those of [4] for unknown reasons.

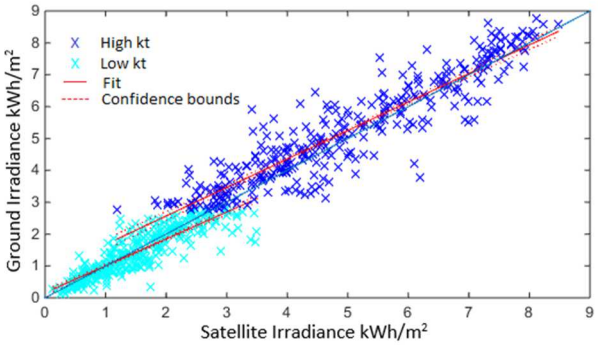

Fig. 3. Scatter plot of daily GHI values of NASA satellite vs ground measurements for Ottawa, Canada. Data is subdivided by clarity index into high and low subsets, with a dividing value set as the median of k_t=0.59.

B. DNI Data Comparison

A data subset of approximately one year of high-availability validated ground-measured DNI (from July 2014 to August 2015) was compared to both version 2.4 (v2.4) and version 3 (v3) from SolarAnywhere® [16], where the ground data was converted from 2 minute resolution into top-of-the-hour averaged data for comparison to the hourly satellite data. The SolarAnywhere v3 model employs new infrared channels and improved algorithms to better differentiate snow and ice from clouds [2]; Ottawa, with its 175 cm average annual snowfall, is thus an ideal ground truth location. The rRMSE and rMBE results given in Table IV indicate that the v3 model significantly improves the agreement, reducing the rMBE from 8.8% to 1.2%, and the rRMSE from 43.9% to 10.9%. The values for v2.4 are similar to those from sporadically cloudy sites in a similar study in California [3], while the agreements for v3 are similar to those found for more northerly US sites [17]. The graphical comparison of v3 versus ground is shown in Fig. 4 where the v3 data shows a strong positive linear correlation without the noticeable outlier subsets seen in the v2.4 comparisons [3, 17].

TABLE IV.
AGREEMENT BETWEEN GROUND MEASURED DNI AND SOLARANYWHERE SATELLITE DNI

	v2.4	v3
rRMSE (%)	43.9	8.8
rMBE (%)	-10.9	-1.2

It is important to study the temporal dynamics of the solar resource since concentrating solar technologies may have non-linear performance with intensity [18]. In Fig. 4, the frequency distributions (counts within 50 W/m^2 bins) and the cumulative distribution functions for the ground, satellite v2, and satellite v3 DNI datasets are shown in blue, red, and dark red, respectively. There is a remarkable disagreement between the ground and satellite datasets for the lowest intensity bin: v2.4 overestimates at the low values, since ice and snow can be mistaken as clouds. With this issue resolved in v3, the v3 dataset exhibits an underestimation of counts in the lowest DNI bin; this is due the geographic averaging effects across a satellite image missing local zero values. For the mid-range bins, from 50 W/m^2 to 750 W/m^2, all three datasets are similar, but v3 has more counts in the 750 to 850 W/m^2 bins while ground data contains more counts in the very high 900 to 100 W/m^2 bins. This discrepancy at the high DNI ranges is also due to the geographic averaging inherent in satellite telemetry data.

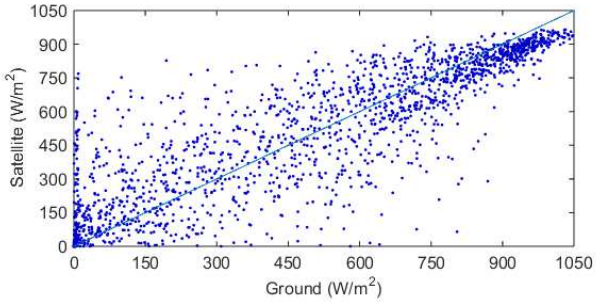

Fig.4. Scatter plot of hourly DNI values of SolarAnywhere satellite v3 versus ground measurements for Ottawa, Canada.

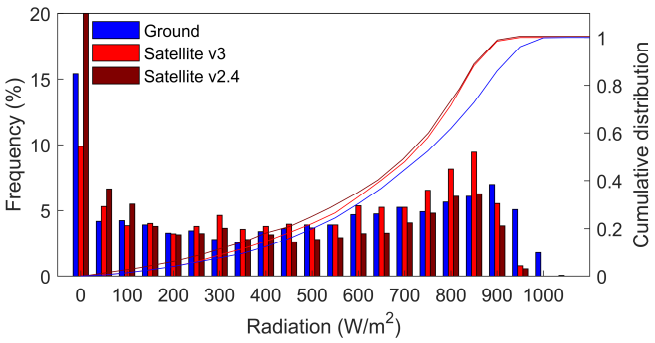

Fig. 5. Frequency distribution of hourly ground and satellite DNI measurements (left axis) with the associated cumulative distribution (right axis).

V. DISCUSSION AND NEXT STEPS

The satellite data's completeness and coverage generally lead it to be the most ameneable source for project energy yield studies. However, our analysis of the frequency distribution of ground vs satellite DNI has shown significant differences in their statistics, which may have an impact in certain situations. We therefore plan to enhance the completeness of our ground dataset by using data from the other instruments to backfill the missing values. This is straightforward using equation (5) if data from any two of the three instruments are available. If data from only one instrument are available, a model appropriately evaluated and

tuning for test site climate conditions must be employed. These backfilled data will have the uncertainty and statistics of ground-based measurements. The resulting complete, site-specific, high temporal granularity dataset will be useful for dynamic analyses.

The multiyear validated and cross-filled data will be made publically available. More extensive analysis of both the GHI and DNI datasets versus SolarAnywhere and other relevant datasets for the Ottawa regions will be undertaken. Furthermore, the SUNLAB has acquired a new high quality instrumentation tracker, with new DNI pyrheliometer, GHI pyranometer and tracked shadow ball for DHI, which will provide further redundancy, accuracy, and increased availability as the datasets are extended in time.

VI. CONCLUSION

A detailed validation and correction methodology has been developed and applied to a multi-year dataset measured by three secondary standard irradiance instruments. By undertaking corrections to instrument responsivities for temperature, cosine and shadowband effects, and by screening for non-tracking and other operational effects, the study was able to prove excellent agreement between the three ground instruments. This paper further found very good agreement between ground and third party GHI and DNI satellite datasets, with mean bias errors less than 2%. One notable difference between ground and satellite measurements was found in the frequency distributions of their respective DNI values, with satellite data underrepresenting both near-to-zero and maximal DNI values due to the averaging effect over the wide geographic coverage spanned by the image resolution. This may be of concern where dynamic performance is critical, so further comparative studies are warrented.

ACKNOWLEDGEMENTS

The authors would like to thank the many members of the SUNLAB team who contributed to the design, build and five year operation of the test site, as well as the strong support of the University of Ottawa Facilities team. The authors also gratefully acknowledge the support from Morgan Solar Inc., the Natural Science and Engineering Research Council of Canada (NSERC), the Ontario Research Foundation, and the Ontario Centres of Excellence.

REFERENCES

[1] Wilcox, S. National Solar Radiation Database 1991 – 2010 Update: User's Manual. (2012).

[2] J. Dise, A. Kankiewicz, J. Schlemmer, K. Hemker, S. Kivalov, T. Hoff, and R. Perez, "Operational improvements in the performance of the SUNY satellite-to-solar irradiance model using satellite infrared channels. *Conf. Rec. IEEE Photovolt. Spec. Conf.* 960–963 (2013).

[3] L. Nonnenmacher, A. Kaur, and C.F.M. Coimbra, "Verification of the SUNY direct normal irradiance model with ground measurements". *Sol. Energy*, 246–258 (2014).

[4] M. Sengupta, "Next-Generation Satellite Modeling for the National Solar Radiation Database", *PV Performance Modeling Workshop*, Cologne, Germany (2015).

[5] R. Djebbar, D. Belanger, D. Boutin, E. Weterings, M. Poirier, "Potential of concentrating solar power in Canada", *Energy Procedia* 49 (2014).

[6] J. Mohammed, M. Yandt, M. Wilkins, A. Muron, T.J. Hall, J.E. Haysom, K. Hinzer, "Collection and Storage of Direct Spectral Irradiance and DNI Datasets with High Temporal Resolution for CPV Energy Yield Assessments", *39th Photovolt. Spec. Conf.* (2013).

[7] V. Tatsiankou, K. Hinzer, H. Schriemer, J. Haysom, R. Beal, "A Novel Instrument for Cost-Effective and Reliable Measurement of Solar Spectral Irradiance", *42th Photovolt. Spec. Conf.* (2015).

[8] I. Reda, "Method to Calculate Uncertainties in Measuring Shortwave Solar Irradiance Using Thermopile and Semiconductor Radiometers", *NREL/TP-3B10-52194*, (2011).

[9] T. Stoffel, D. Renne, D. Myers, S. Wilcox, M. Sengupta, R. George, C. Turchi, "Concentrating Solar Power: Best Practices Handbook for the Collection and Use of Solar Resource Data", *NREL/TP-550-47465* (2015).

[10] A. Skartveit, J.A. Olseth, and M.E. Tuft, "An hourly diffuse fraction model with correction for variability and surface albedo", *Sol. Energy*., 63 173-183, (1998).

[11] G. Sanchez, A. Serran, M.L. Cancillo, and J.A. Garcia, "Comparison of shadow-ring correction models for diffuse solar irradiance", *J. Geophys. Research* 117, D09206 (2012).

[12] F.J. Batlles, F.J. Olmo, and L. Alados-Arboledas, "On shadow band correction methods for diffuse irradiance measurements", *Sol. Energy*, 54, 105–114 (1995).

[13] R. Djebbar, r. Morris, D. Thevanard, R. Perez, and J. Schlemmer, "Assessment of SUNY version 3 global horizontal and direct normal solar irradiance in Canada", *En. Procedia*, 30 1274-1283, (2012).

[14] NASA Langley Research Center Atmospheric Science Data Center Surface meteorological and Solar Energy (SSE): https://eosweb.larc.nasa.gov/sse/ and via RETScreenPlus: http://www.retscreen.net/ang/home.php.

[15] K. de Brabandere, "Evaluation of Satellite irradiance data at 200 sites in Western Europe", *PV Performance Modeling Workshop*, Oct. 22-23 Cologne, Germany (2015).

[16] SolarAnywhere® is a database of solar irradiance and associated data, ©2008-2010 by Clean Power Research; https://solaranywhere.com/Public/About.aspx.

[17] J.L. Bosch, A. Kankeiwicz, J. Dise, J. Schlemmer, K. Hemker, S. Kivalov, and R. Perez, "SUNY Satellite-to-Solar Irradiance Model Improvements", *Clean Power Res. Report* (2015).

[18] C.A. Gueymard, "Direct Normal Irradiance for CSP/CPV: Modeling Challenges", *Int. Solar En. Society webinar* (2013).